8th Biennial International Conference
& Exposition on Petroleum Geophysics

"HYDERABAD 2010"

P-107

Seismic attributes and property estimation of thin sub-resolution sand-shale reservoirs

Piyapa Dejtrakulwong, *Stanford Rock Physics Laboratory, Stanford University*
Tapan Mukerji*, *Stanford Center for Reservoir Forecasting, Stanford University*
Gary Mavko, *Stanford Rock Physics Laboratory, Stanford University*

Summary

Property estimation of thin sand-shale reservoirs using seismic response could be challenging due to limited seismic resolvability. A forward-modeled investigation on seismic signatures of multiple realizations of pseudo 1-D thin sand-shale sequences, constructed from a discrete, first order Markov chain model, reveals possible distinctions of thin sand-shale reservoirs with different net-to-gross and saturations in the wavelet-transform-based attribute space. We also show a numerical example of how to apply this technique in a real situation. First, we assume that the transition matrix or thickness distributions at the well location are known. In reality, this information can be estimated from the well data. Then, we create synthetic 2-D spatial models describing geology away from the well, explore statistically how attributes would vary with a change of sand/shale ratios and apply the statistics to obtain the posterior distributions of net-to-gross at three selected locations from the seismic section.

Introduction

Seismic estimation of reservoir properties is common in petroleum exploration. However, detecting and estimating petrophysical properties of thinly layered reservoirs with layers below seismic resolvability can be challenging. Most studies of thin beds and their seismic response have focused on the resolution problem (e.g. Chung and Lawton, 1995; Okaya, 1995). Lange and Almoghrabi (1988) introduced lithology and pore fluids in their forward modeling of thin layers and suggested that spectral parameters could help discriminate layer properties. However, the study was limited to a layer bounded by two different materials with fixed properties.

Most stratigraphic sequences in nature reflect non-random stacking sedimentary patterns. Depending on depositional environments, the main characteristics of such patterns include lateral extents, vertical arrangements of lithologies, layer thickness distributions, etc (Harms and Tackenberg, 1972). Two stacks of sand-shale layers with similar average properties can yield different seismic response if layer arrangements are different (e.g. lamination, finingupwards) (e.g. Khattri and Gir, 1976; Takahashi, 2000; Hart, 2008). Markov chains have been used as a tool to simulate bedded sequence to capture these preferred directionality and asymmetric facies associations signaling depositional process (e.g. Krumbien, 1969; Harbaugh and Bonham-Carter, 1970; Schwarzacher, 1975; Xu and MacCarthy, 1996; Parks et al., 2000). Velzeboer (1981) modeled sequences by a first-order Markov chain with distributions of physical properties and theoretically showed possible estimation of sand-shale ratios from power spectrum of reflected response. Sinvhal and Sinvhal (1992) constructed transition matrices from well logs using firstorder Markov chains to simulate pseudologs. Realizations of synthetic seismograms were created and used in statistical studies for lithology discrimination.

The main focus of this paper is to study seismic signatures of multiple realizations of thin sand-shale sequences. A sedimentary column is generated in two steps: simulating the arrangements of lithology by running a Markov chain and assigning physical properties corresponding to each layer from rock-physics relations. Layer properties assigned to the sequences come from established rockphysics binary-mixture models. Forward computation of the seismic response of the sequences is then used to extract statistical attributes and relate them to the spatial patterns and properties of thin sand-shale reservoirs.

Markov Chain Models in Stratigraphic Sequences

In stratigraphic analysis, a column of sediments can be described as a spatial arrangement of a finite number of discrete states (i.e. lithology). Markov chains provide a mathematical tool utilizing concepts of conditional probabilities to describe the dependency of the current state (i.e. lithology) on the previous states. If the transition from one state to the next depends only on the immediately preceding state, the chain is said to be first-order (Harbaugh and Bonham-Carter, 1970; Sinvhal and Khattri, 1983). Transition probability values for every state pair are tabulated into a transition matrix, which is a common method of representing a Markov-chain model (Parks et al, 2000). An element p_{ij} (at the i^{th} row and j^{th} column) represents the probability of a transition from state i to state j, or the probability of going to state j, given that i is the current state. In a stratigraphic study, the transition matrix is usually obtained from real geological observations and can be constructed in two common ways: counting states using a fixed sampling interval, or counting states only when a transition occurs (an embedded form). For the former approach, the lithologic state is determined and considered only at discrete points equally spaced along a stratigraphic column. This allows successive points to have similar lithology, meaning the diagonal element (i.e. probability that a state has a transition to itself) can be nonzero (Krumbein and Dacey, 1969). In practice, selecting a proper sampling interval for this method can be problematic. Choosing an interval too small relative to the overall average bed thickness can increase the counts of transitions of a state to itself. Consequently, the diagonal elements become very large, and probabilities of the state transiting into the others become unreasonably small. In contrast, using too large a sampling interval can miss very fine-layered characteristics of the sequences (Sinvhal and Sinvhal, 1992). Krumbein and Dacey (1969) observed that the lithologic state of a sequence simulated by these kind of chains often yields thicknesses that are geometrically distributed.

In our simulation, we discretize the lithology into 4 states representing a gradual increase in shaliness. Following the method of fixed sampling by using a step size of 0.5 m, we create 4x4 transition matrices whose states are sand, shaly sand, sandy shale, and shale. Basic geological patterns such as aggrading, fining upwards, and coarsening upwards sequences can be simulated by matrices with appropriate off-diagonal patterns as shown in the examples in Figure 1. In contrast, in an embedded-form transition matrix, all diagonal elements are zero, since transitions are considered only when lithologic states change. In this case, thickness distributions are extracted directly from geological observations (Figure 2).

Rock physics relations for sand-shale mixtures

A set of rock-physics relations used in our simulations includes the Yin-Marion mixing model (Marion et al., 1992), the soft sand model (Avseth et al., 2005), and Gassmann's fluid substitution equation (Gassmann, 1951). Marion et al. (1992) introduced a dispersed-mixing model for bimodal mixtures, in which the two end-members are particles of two different sizes. In this case, we consider sand-shale mixtures where sand grains are mixed with clay particles. The model then describes the topology of the mixing and relations between volume fraction of clay and porosity. For clay fraction less than the sand porosity, clay starts filling the sand pore space. Sand grains provide the load-bearing matrix of the mixture. At this stage, porosity decreases because clay particles replace some portions of the original sand pore space. When the clay content is greater than the sand porosity, sand grains are displaced and disconnected. The transition from grain-supported to clay-supported sediments occurs. At this stage, porosity increases linearly with increasing clay fraction because the situation is simply equivalent to substituting voidless sand grains with a porous chunk of clay (Yin, 1992). Thus, the plot of fraction of clay versus porosity shows a V-shape pattern (Figure 3).

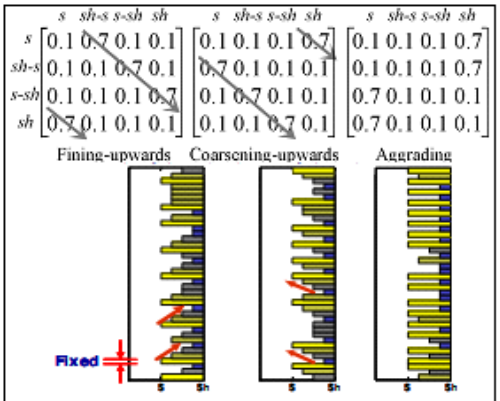

Figure 1: Examples of transition matrices with fixed sampling intervals. Three different types of geology are shown: fining upwards, coarsening upwards, and aggrading sequences. In this case, lithologic states are sand (s), shaly sand (sh-s) sandy shale (s-sh) and shale (sh). The off diagonal elements marked by arrows control the directionality of the sequences.

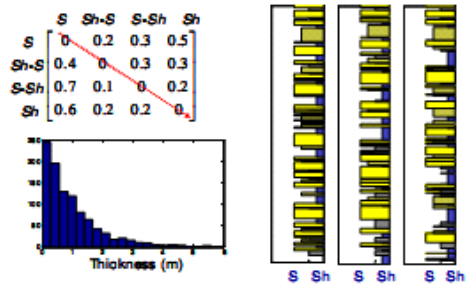

Figure 2: Examples of an embedded-form transition matrix with realizations of sequences. In this case, lithologic states are sand (s), shaly sand (sh-s) sandy shale (s-sh) and shale (sh). An example of thickness distributions used is shown in the lower left.

We assign mean clay fractions of 0.1, 0.3, 0.6 and 0.9 to the sand, shaly-sand, sandy-shale and shale states respectively. The corresponding porosity values are determined from the Yin-Marion model. Mean velocity is obtained from the soft sand model which uses the lower Hashin-Shtrikman bound to construct velocity-porosity trends for sand mixing with varying clay content (Avseth et al., 2005). Density is a weighted average of density of each component in the layer including pore fluids. We introduce uncertainties by assuming each lithology state having a distribution of velocities with a mean equal to the calculated velocities and standard deviations of 0.1–0.2 km/s.

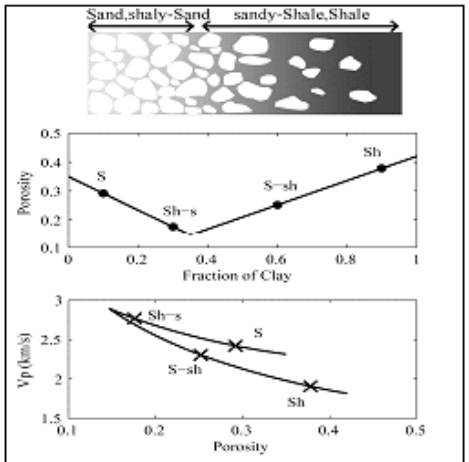

Figure 3: Illustrations of sand-shale mixtures, with their porosity and velocity values related to clay content (Modified after Marion, 1992). Porosity vs. clay content shows a V-shaped trend, where the two end points are the pure sand and pure shale porosity. Four lithologic states are marked including sand (s), shaly-sand (sh-s), sandy-shale (s-sh) and shale (sh).

Two main scenarios are explored. First, to investigate effect of net-to-gross, we study a set of aggrading-type transition matrices with same water saturation (Sw=0.1 for sand layers and Sw=1 for the others) but with different limiting distributions (i.e. varying sand fractions). For this scenario, we run simulations for velocity distributions with standard deviations of 0.1 and 0.2 km/s. Second, to study the effect of saturation, we focus on sequences generated from a similar transition matrix but with varying saturation values. We use Gassmann's equation to substitute mixtures of water and oil with the desired saturations into the sand layers in the sequences. All other lithologies have Sw equal to 1. Full waveform, normally-incident, reflected seismograms (Figure 4) are simulated using the Kennett algorithm (Kennett, 1983) with a 30-Hz Ricker wavelet.

Wavelet–transform based analysis

Wavelet transform decomposes a signal into a set of scaled and translated versions of a selected wavelet function. The transform has been used, e.g, to study fractal behavior of seismic data and well logs to characterize lithofacies (Álvarez et al., 2003; López and Aldana, 2007). Using well logs, López and Aldana (2007) showed a possible relation

of lithofacies and parameters including fractal dimension, intercept and slope obtained from linear fits to plots of logvariance of wavelet-transform coefficients versus scale. Using a complex Gaussian wavelet, we wavelet transform the simulated seismograms yielding transform coefficients at various scales. We calculate variance of the modulus of these coefficients for every scale and make a log-log (base2) plot of the variance versus scale (Figure 5). Then, we extract the slope and intercept of a linear fit as statistical attributes for each realization.

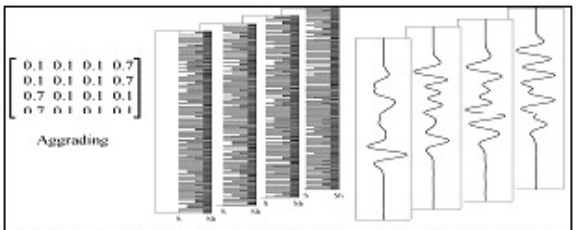

Figure 4: Examples of generated seismic response for multiple realizations of sequences.

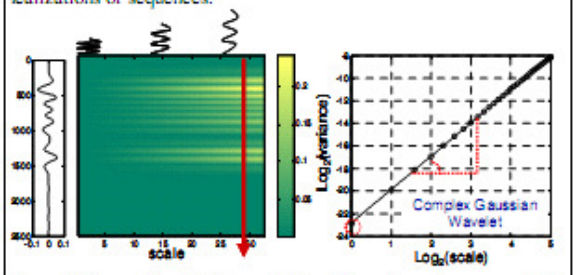

Figure 5: Example plot of wavelet transform of a seismogram (left) and plot of log (scale) versus log (variance of modulus of wavelet-transform coefficients) and the linear fitting curve.

Results

Figure 6 shows slope versus intercept from wavelet transforms of seismic responses of sequences from 6 different transition matrices of the form. shown in Table 1. However, their limiting distribution (π) are different (i.e. sand proportion, π_{sand}, varies from 0.32 to 0.48). In all sequences, all sand layers have water saturation (Sw) of 0.1 while other lithology states have Sw of 1. Two plots correspond to results from simulations using two standard deviations (σ_v= 0.1 and 0.2 km/s) for velocity distributions. In both cases the clouds of points move down toward the lower left when π_{sand} increases as the transition matrices change. However, for a larger σ_v (e.g. σ_v= 0.2 km/s), points corresponding to different π_{sand} vare less spread out. The probability distributions of slope and intercept are plotted in Figure 7. Both slope and intercept distributions move toward the left as π_{sand} increases. Figure 8 illustrates changes in slope and intercept as water saturations in the sand layers vary (Sw=0.1, 0.5, and 1). All three transition matrices have the same π : [0.45 0.05 0.05 0.45]. Data points, especially those corresponding to Sw=1, are gradually separated out as we move from the leftmost to the rightmost plots, due to changes in intercept (Figure 9).

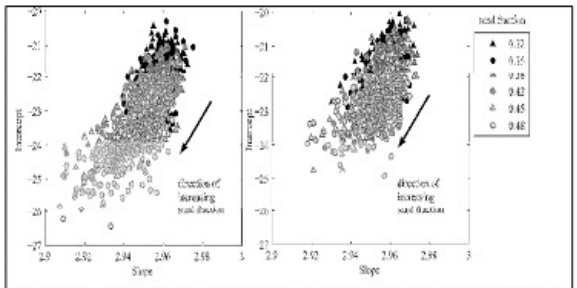

Figure 6: Plot of slope and intercept of wavelet transforms of seismic responses for 2 different standard deviations of velocities: (Left) 0.1 km/s and (Right) 0.2 km/s. Points correspond to sets of 200 Monte Carlo simulations generated from different transition matrices with various sand fractions (πsand). Sw is 0.1 for sand layers and 1 for the others.

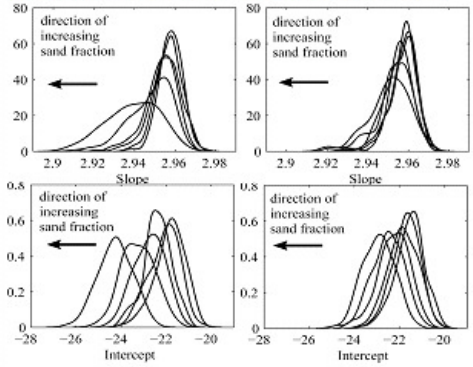

Figure 7: Probability distributions of slope and intercept values corresponding to data points in Figure 6 for both values of standard deviations. The direction of increasing sand fractions (πsand) is to the left for all plots.

Table 1: Transition matrices used to generate sequences for simulations in Figure 6. Values of x used are from 0.45 to 0.95.

	Sand	Shaly Sand	Sandy Shale	Shale
Sand	(1 - x)/3	(1 - x)/3	(1 - x)/3	x
Shaly Sand	(1 - x)/3	(1 - x)/3	(1 - x)/3	x
Sandy Shale	x	(1 - x)/3	(1 - x)/3	(1 - x)/3
Shale	x	(1 - x)/3	(1 - x)/3	(1 - x)/3

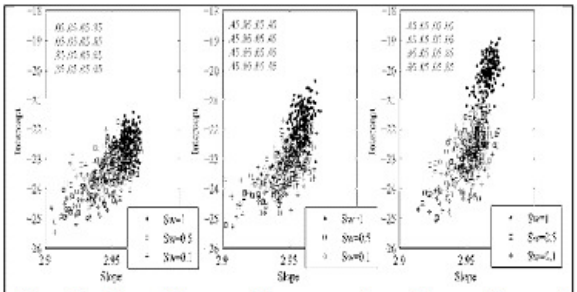

Figure 8: Plot of slope and intercept of wavelet transforms of seismic response for sequences generated by 3 different transition matrices. All matrices have a similar limiting distribution: [0.45 0.05 0.05 0.45]. Different values of water saturation in the sand layers (i.e. Sw=0.1, 0.5 and 1) are shown in the legend.

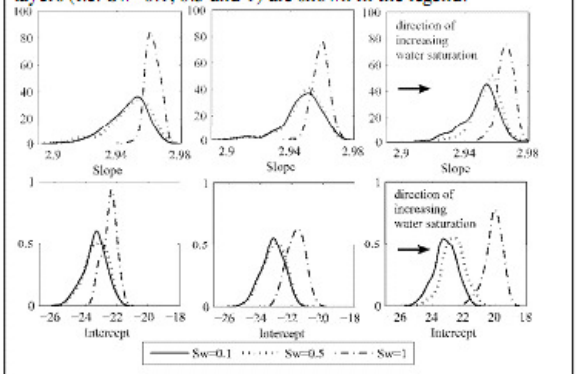

Figure 9: Distributions of slope and intercept values corresponding to the 3 transition matrices in Figure 8 in the same order from left to right.

Discussion

The layer thickness used in our simulations have wavelength to thickness ratio of about 100. Seismic waves cannot distinguish the boundaries of these thin layers because of their band-limited characteristics. Hence, interpretations of these sub-resolution layers can only be based on statistical attributes of the seismograms. In the present study, synthetic seismograms of thin sand-shale sequences are investigated by extracting slope and intercept from a linear fit to the log-log plot of variance of wavelet coefficient modulus versus scale.

We see a decrease in both slopes and intercepts when the percent of sand in the total sequence (π_{sand}) increases for the selected form of transition matrices. For a larger standard deviation (σ_v) used in velocity distributions, we see slopes and intercepts for different π_{sand} are less spread out. One reason for this could be using larger σ_v would result in larger overlaps in velocities drawn for each state. Thus, even when π_{sand} increases (i.e. more sand layers in the sequences), there is not much change in the overall velocities drawn for each sequence because all four lithology states would yield close values of velocities. Larger overlaps in the slope-intercept attributes would also result in larger uncertainties in property estimations.

In some cases, slope and intercept of sequences obtained from the same transition matrix increase with increasing water saturation. It can be seen that different transition matrices can lead to different behavior in the slope intercept space, even when they have the same limiting distribution. The different behavior of the three plots in Figure 8 possibly comes from blockier nature of the sequences generated from the transition matrix in the rightmost plot compared to the left ones. This blocky characteristic is expected since the matrix has two large probabilities in the main diagonal ($p_{ss} = p_{shsh} = 0.85$). Thus, spatial statistics play a critical role in seismic signatures of sub-resolution systems.

This study does not focus on investigating all possible transition matrix configurations; however, the study can be applied to the problem of thin reservoir characterization. Assuming that the stratigraphy in the explored area demonstrates a lateral continuation within conformable sequences, inferred transition matrix from a calibration well could be used to explore statistically how the seismic attributes (in this case, slope and intercept attributes) would change with varying sand/shale ratios and saturations. These statistics of the attributes can then be applied to observations away from the well to help characterize the area and estimate the uncertainties. We show a numerical example of this application in the next section.

Net-to-gross estimation using Bayesian framework

We set up a numerical example by first assuming a known transition matrix estimated at the well location. We use the embedded-form transition matrix with 2 lithologic states representing sand and shale and assume the thickness distribution of both lithologic states to be exponentially distributed with average thickness of 0.3 and 0.5m respectively. These transition matrices and thickness distributions are used to generate 1-D vertical sequences at the well location. Then, we create multiple realizations of 2-D spatial models describing geology away from the well location (i.e. sand layers are thinning linearly starting from the well location into an area away from the well) (Figure 10). We then explore statistically how attributes vary with changes in sand/shale ratios as shown in Figure 11. These statistics will then be applied to a synthetic seismic section for estimating net-to-gross of the area away from the well.

We estimate posterior distributions of net-to-gross at three selected locations from the seismic section. Posterior distributions of net-to-gross given attributes can be obtained using Bayes' formula (Equation 1):

$$P(NG \mid A) \propto P(A \mid NG) \cdot P(NG), \qquad (1)$$

where NG is net-to-gross, A represents attributes, which are slope and intercept in this case, $P(NG)$ is the prior probability, $P(A \mid NG)$ is the likelihood function, and $P(NG \mid A)$ is the posterior probability. In this example, we use a simple geological model (i.e. thinning of sand layers) to create many realizations of 2-D rock sections. From these realizations, we can then estimate $P(NG)$ or the prior probability of net-to-gross and use it together with the likelihood function to obtain the posterior distribution of net-to-gross at three locations as shown in Figure 12. The posterior distribution captures the true value as well as the uncertainty of the interpretation.

Conclusions

An investigation of synthetic seismograms from thin subresolution sand-shale reservoirs is performed. The thinlayer sequences are generated from a set of transition matrices representing aggrading clastic sequences. Wavelet-transform based attributes (slope and intercept in variance-scale plot) are extracted. For the selected form of transition matrices with the same water saturation, an increase in percent of sand (net-to-gross) results in a decrease in both slope and intercept values. For the same transition matrix, an increase in water saturation may result in an increase in both slope and intercept. The present study also shows that not all transition matrices with a similar limiting distribution give the same trends. We show a numerical example of how the wavelet-transform attributes can be used to estimate properties of thin sand-shale reservoirs away from the well. Using Monte-Carlo simulations and Bayes' formula, posterior distributions of net-to-gross for the seismic section can be obtained. Prior geological knowledge about the area can help reduce uncertainty. Further investigation of other attributes will also help us better characterize properties and patterns in thin sand-shale reservoirs.

Acknowledgements

This work was supported by the SRB and SCRF. We also would like to thank Paul Switzer for his suggestions.

References

Álvarez, G., Sansó, B., Michelena, R.J. and Jiménez, J.R., 2003. Lithologic Characterization of a Reservoir Using Continuous-Wavelet Transforms: IEEE Trans. on Geoscience and Remote Sensing, **41(1)**.

Avseth, P., Mukerji, T. and Mavko, G., 2005. Quantitative Seismic Interpretation, Cambridge.

Chung, H. and Lawton, D.C., 1995. Frequency Characteristics of Seismic Reflections from Thin Beds: Canadian J. of Explr. Geophysics, **31**, 32-37.

Dvorkin, J. and Gutierrez, M.A., 2002. Grain Sorting, Porosity, and Elasticity: Petrophysics, **43(3)**, a3.

Flórez, J. and Mavko, G., 2003. Porosity-Velocity Distribution in Stratigraphic Sequences: The MarionYin Model, Search and Discovery, no. 40105.

Gassmann, F., (1951). Uber die elastizitat poroser medien: Vier Natur Gesellschaft, **96**, 1-23.

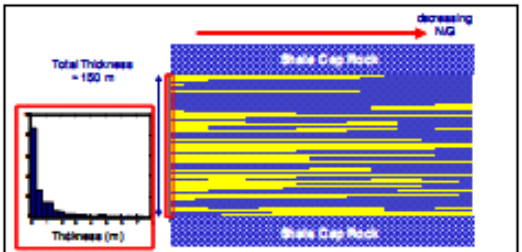

Figure 10: A realization of 2-D geologic section used in the numerical example. The area at the left end marked with the red box corresponds to the well location. Sand and shale are colored in yellow and blue respectively. The thicknesses of sand layers decrease linearly away from the well. The total thickness of reservoir is 150 m. An example of the thickness distribution used to simulate the sequence at the well location is also shown.

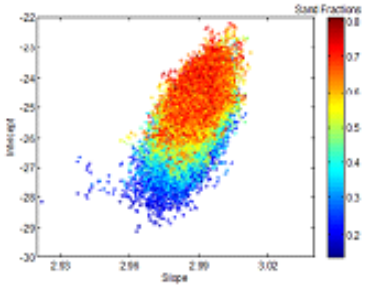

Figure 11: Results of 1000 realizations of 2-D sections show how slope and intercept vary with varying sand fractions.

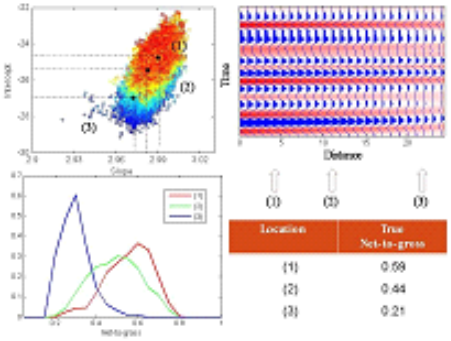

Figure 12: (Lower left corner) Posterior probability distributions of net-to-gross for three selected locations on the unknown seismic section labeled as (1), (2) and (3). The true values for each location are shown in the table at the lower right corner.

Harbaugh, J.W. and Bonham-Carter, G., 1970. Computer Simulation in Geology, Wiley.

Hart, B. (2008) Stratigraphically Significant Attributes: The Leading Edge, March 2008, 320-324.

Khattri, K. and Gir, R., 1976. A Study of the Seismic Signatures of Sedimentation Models Using Synthetic Seismograms: Geophysics, **34**, 454-477.

Krumbein, W.C. and Dacey, M.F., 1969. Markov Chains and Embedded Markov Chains in Geology: Mathematical Geology, **1(1)**, 79-96

Lange, J. and Almoghrabi, H., 1988. Lithology Discrimination for Thin Layers Using Wavelet Signal Parameters: Geophysics, **53(12)**, 1512-1519.

López, M. and Aldana, M., 2007. Facies Recognition Using Wavelet Based Fractal Analysis and Waveform Classifier at the Oritupano-A Field, Venezuela: Nonlinear Processes in Geophysics, **14**, 325-335.

Marion, D., 1990. Acoustical, Mechanical and Transport Properties of Sediments and Granular Materials, Ph.D. Thesis, Stanford University.

Marion, D., Nur, A., Yin, H. and Han, D., 1992. Compressional Velocity and Porosity in Sand-Clay Mixtures: Geophysics, **60(1)**, 241-251.

Okaya, D.A., 1995. Spectral Properties of the Earth's Contribution to Seismic Resolution: Geophysics, **60(1)**, 241-251.

Parks, K.P., Bentley, L.R. and Crowe, A.S., 2000. Capturing Geological Realism in Stochastic Simulations of Rock Systems with Markov Statistics and Simulated Annealing: Journal of Sedimentary Research, **70(4)**, 803-813.

Schwarzacher, W., 1975. Sedimentation Models and Quantitative Stratigraphy, Elsevier.

Sinvhal, A. and Khattri, K., 1983. Application of Seismic Reflection Data to Discriminate Subsurface Lithostratigraphy: Geophysics, **48(11)**, 1498-1513.

Sinvhal, A. and Sinvhal, H., 1992. Seismic Modeling and Pattern Recognition in Oil Exploration, Kluwer Academic Publishers.

Takahashi, I., 2000. Quantifying Information and Uncertainty of Rock Property Estimation from Seismic Data, Ph.D. Thesis, Stanford University.

Velzeboer, C.J., 1981. The theoretical Seismic Reflection Response of Sedimentary Sequences: Geophysics, **46(6)**, 843-853.

Xu, H. and MacCarthy, A.J., 1996. Markov Chain Analysis of Vertical Facies Sequences Using a Computer Software Package (SAVFS): Courtmacsherry Formation (Tournaisian), Southern Ireland: Computers & Geoscience, **24**, 131-140.

Yin, H., 1992. Acoustic Velocity and Attenuation of Rocks: Isotropy, Intrinsic Anisotropy, and Stress Induced Anisotropy, Ph.D. Thesis, Stanford University.